Project No. 11-3095

Rapid Computer Aided Ligand Design and Screening of Precious Metal Extractants from TRUEX Raffinate with Experimental Validation

Fuel Cycle

Aurora (Sue) Clark
Washington State University

In collaboration with:
None

Jim Bresee, Federal POC
Dean Peterman, Technical POC

NEUP Nuclear Energy University Programs
U.S. Department of Energy

Final Report: Rapid Computer Aided Ligand Design and Screening of Precious Metal Extractants from TRUEX Raffinate with Experimental Validation

PI: Aurora Clark (Washington State University)

CO-PI: Nathalie Wall, Paul Benny (WSU)

I. Introduction

Rhodium is the most extensively used metal in catalytic applications (i.e., oxidation of ammonia to nitric acid, automobile catalytic converters) and occurs in mixed ores with platinum group metals (PGMs) in the earth's crust in low concentrations (0.4 - 10 ppb).[1-4] It is resistant to aerial oxidation and insoluble in all acids, including aqua regia making classical purification methods time-consuming and inefficient.[1, 4-6] To ensure adequate purity, several precipitation and dissolution steps are necessary during separation.[1] Low abundance, high demand, and extensive processing make rhodium the most expensive of all PGMs. From alternative sources, rhodium is also produced in sufficient quantities (0.47 kg per ton initial heavy metal (tIHM)) during the fission of U-235 in nuclear reactors along with other PGMs (i.e., Ag, Pd, Ru).[3, 7] A typical power water reactor operating with UO_2 fuel after cooling can generate PGMs in quantities greater than found in the earth's crust (0.5-2 kg/tIHM).[7] This currently untapped supply of PGMs has the potential to yield $5,000-30,000/tIHM.[8] It is estimated that by the year 2030, the amount of rhodium generated in reactors could exceed natural reserves.[3] Typical SNF processing removes the heavier lanthanides and actinides and can leave PGMs at ambient temperatures in aqueous acidic (Cl^- or NO_3^-; pH < 1) solutions at various activities.[9] While the retrieval of these precious metals from SNF would minimize waste generation and improve resource utilization, it has been difficult to achieve thus far.

Two general strategies have been utilized to extract Rh(III) from chloride media: ion pairing and coordination complexation.[14] Ion pairing mechanisms have been studied primarily with the tertiary and quaternary amines.[15-19] Additionally, mixed mechanism extractions have been observed with N-n-octylaniline[15] and sulfoxides[20, 21] in which ion pairing is the initial mechanism, and longer extraction equilibrium time generated coordination complexes. Very few coordination complexation extraction ligands have been studied. Within this project we approached this problem to this problem through the design of a software program that uses state-of-the-art computational combinatorial chemistry and is developed and validated with experimental data acquisition; the resulting tool allows for rapid design and screening of new ligands for the extraction of precious metals SNF. Herein we describe the software that has been produced, ligands that have been designed, and fundament new understandings of the extraction process of Rh(III) as a function of solution phase conditions (pH, nature of acid, etc.)

II. Work Products

1) Peer-reviewed publications:

Rh(III) extraction by phosphinic acids from nitrate media. Alex C. Samuels, Emily M. Victor, Nathalie Wall, Aurora E. Clark. *Solvent Extraction and Ion Exchange. 33(4), 418-428* ***(2015)*** *DOI: 10.1080/07366299.2015.1005535*

Integrated Computational and Experimental Protocol for Understanding Rh(III) Speciation in Hydrochloric and Nitric Acid Solutions. Samuels A. , Boele C. , Bennett K., Clark

S.B., Wall N.A, Clark A.E. *Inorganic Chemistry.* 53(23), 12315-12322 ***(2014)***. *DOI: 10.1021/ic501408r*

Recovery of rhodium with a novel soft donor ligand using solvent extraction techniques in chloride media. Shalina C. Bottorff, Ashton S. Powell, Thomas R. Hayes, Aurora E. Clark, Stephen Mezyk, Paul D. Benny. *Inorganic Chemistry*, In Preparation, **2016**.

Solvent extraction of rhodium(III) from chloride or nitrate media by N,N-diethyl-N'-benzoylthiourea. *Dalton Transaction*, In Preparation, **2016**.

2) Conference Proceedings

Media Effects on the Recycling of Rhodium From Spent Nuclear Fuel. Shalina C. Bottorff, Ashton S. Powell, Thomas R. Hayes, Aurora E. Clark, Stephen Mezyk, Paul D. Benny. *Waste Management* **2016**.

3) Theses:

Investigating the speciation and extraction of commercially important metals from spent nuclear fuel raffinates: an integrated computational and experimental approach. Alex C. Samuels. *Ph.D. Dissertation. Washington State University, Pullman **(2014)***.

Speciation, separation, and solvent extraction of rhodium. Cherilynn A. Boelé. *Master. Washington State University, Pullman **(2014)***.

Ligand and material design for the recovery of transition metals (Rh, Tc) from spent nuclear fuel. Shalina Bottorff, *Ph.D Dissertation. Washington State University, Pullman (**2016** anticipated).*

4) Conference presentations:

Extraction of rhodium (III) by organophosphorus compounds in conditions relevant to nuclear waste: A combined experimental and computational approach. Alex Samuels, Aurora E. Clark, Nathalie A. Wall. Dr. William R. Wiley Research Exposition, WSU Pullman, WA 02/21/2014

Examination of Rh(III) Speciation in Acidic Media. Alex Samuels, Cherilynn A. Boele, Aurora E. Clark, Nathalie A. Wall. 37th Annual Actinide Separations Conference. Spokane, WA 06/24-27/2013

The extraction of rhodium with relevance to the PUREX and TRUEX process. Cherilynn A. Boele and Nathalie Wall. Puget Sound Women Chemists Retreat, Vancouver, BC, Canada, 05/30-06/01/2014

Media Effects on the Recycling of Rhodium From Spent Nuclear Fuel. Shalina C. Bottorff, Ashton S. Powell, Thomas R. Hayes, Aurora E. Clark, Stephen Mezyk, Paul D. Benny. *Waste Management 2016*.

5) Awards:

Alex Samuels: College of Arts and Sciences Graduate Achievement Award in the Sciences at the Doctoral Level (2014)

6) Disclosures for Patent/Licensing: Computationally Assisted Design of Metal Extractants, Aurora E. Clark, WSU, (2014).

III. Scientific Accomplishments

III.a Software Development – Computationally Assisted Design of Metal Extractants (CADME).

The fundamental approach for the software design of CADME is to create a gateway that interfaces and launches existing software programs to: 1) create large databases of candidate ligands for extraction, and 2) refines the database through a series of systematically higher accuracy calculations of known metrics for ligand design (including ligand reorganization energies, and ligand-metal binding energies). As for part (1) CADME is interfaced with the HOSTDESIGNER program out of OakRidge National Laboratory, which can create a ligand database of all potential ligands that can be created from user supplied building blocks. CADME first reads in the ligand database created by HOSTDESIGNER and then, the user chooses a computational work-flow for the screening process. The work-flow consists of either single-point of geometry optimization calculations, whereupon energy differences are used as the initial metrics for screening. For example, the first step in the workflow may be to calculate the ligand reorganization energy needed for the ligand to bind to a given metal. An energy threshold is chosen by the user to filter out ligands whose reorganization energy is too large to be considered to easily bind to the metal. The second step in the workflow may be to calculate the ligand binding energy to the metal. Again, a threshold criterion is chosen that filters out ligands that are not strongly bound to the metal. The code is versatile enough to have as many steps in the workflow as the user desires. Other algorithms have also been implemented to help handle the large data-sets employed. For example, a graph theoretical fingerprinting algorithm was implemented to create a numerical score for each ligand that is based upon the coordination environment that the ligand adopts about the metal. In this way, we can dynamically keep track of how the coordination environment is correlated to ligand binding energy. CADME can interface with the NWChem software to launch the energy and optimization calculations using whatever computational approach deemed suitable for the particular system, though it is generally anticipated to be some form of density functional theory or perturbation theory.

As illustrated in Figure 1, the original version of CADME, described above, is now being extended to be coupled with statistical mechanical codes that can begin to understand how solvent organization about the metal-ligand complex could be related to the end distribution coefficient. In this particular project, as it pertains to precious metal or platinum group extraction, it is of paramount importance to know what the reacting species are that the ligand will be reacting with. As such, one of the first experimental studies undertaken was to understand the speciation of Rh(III) in chloride and nitric acid media relevant to SNF raffinates.

Figure 1. Workflow of CADME software program and filtering processes that can be involved for both the original version (V.1) and the in-development version 2 (V.2).

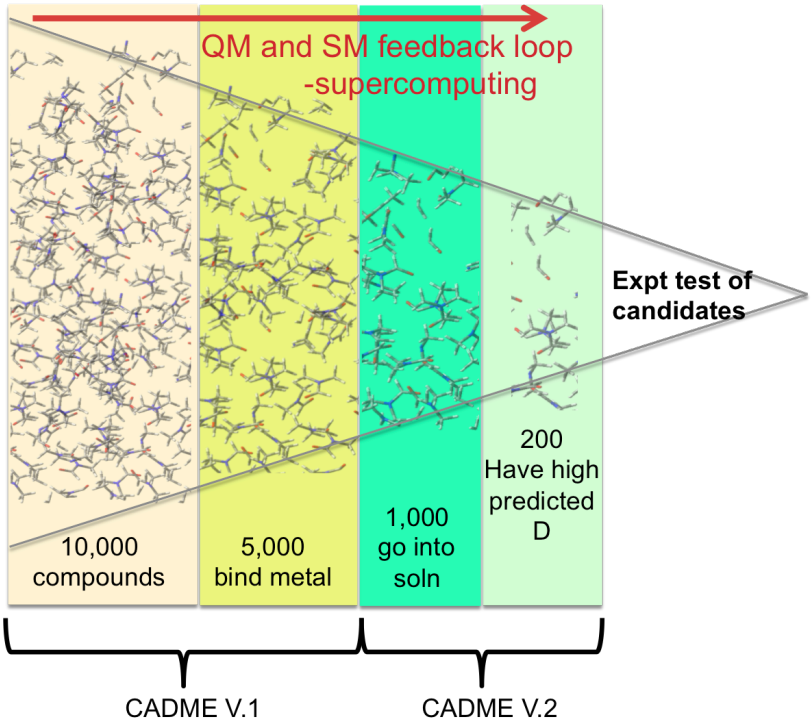

III.b Speciation of Rh(III) in Chloride and Nitrate Media *(Inorganic Chemistry* ***2014*** *53, 12315-12322)*

Rh is quite stable in the trivalent oxidation state; however, the speciation kinetics in chloride media is particularly complicated. The completely aquated hexa-aquarhodium(III), $[Rh(H_2O)_6]^{3+}$, the hexachloridorhodate(III), $[RhCl_6]^{3-}$, and all mixed aqua/chlorido complexes, including isomers, ($[RhCl_x(H_2O)_{6-x}]^{3-x}$ with x = 1 - 5) can exist simultaneously in solution. At high chloride concentrations and millimolar Rh(III) concentrations, a dimer, $[Rh_2Cl_9]^{3-}$, has been reported to form. Further adding to the variety of complexes possibly present are chloride and oxygen bridged polymeric Rh species, of which very little is known. The formation of polymeric species is not unique to Rh(III) and is observed with Cr(III) and Fe(III), where the pH < 7 and metal concentrations of ≥ 10^{-3} M. The concentration of each complex depends primarily on the chloride concentration, but also, to a lesser degree, on the temperature, age, and pH of the solution. For example at pH > 2.9, the aqua/chlorido complexes are believed to undergo hydrolysis to form $[RhCl_4(OH)(H_2O)]^{2-}$. As a result of the complicated species distribution in solution, study of the chlorido-aqua species has relied upon purification of a specific species of interest via ion exchange chromatography, followed by characterization using polarography and/or ultraviolet-visible (UV-Vis) spectroscopy (focusing upon the low-energy portion of the spectrum, λ ≥ 300 nm). Significant efforts have been devoted to understanding the mechanistic aspects of aquation reactions of various chlorido-aqua species. In principle, speciation under

varying chloride concentrations should be straightforward to determine provided the binding constants of all potential molecular species; however, the available speciation diagrams are suspect as different interpretations of the polarographic data yield a range of binding constants. Even less is understood about the speciation of Rh(III) in nitric acid media, as nucleophilic substitution of chloride by nitrate has been observed.

Examination of Rh speciation under conditions relevant to extraction from raffinates is necessary to design extraction protocols for this metal from spent fuel. To aid in the assignment of species within solution and to understand the potentially intricate distribution and dynamic nature of species, modern studies can take advantage of computational chemistry to understand the thermodynamic favorability for the formation as well as the prediction of the UV-Vis spectra of individual entities. The goal of this work is twofold: first, to investigate Rh(III) speciation in acidic media under conditions that are relevant to separations applied to spent fuel raffinates, and second, to demonstrate that the speciation can be understood through a combined experimental and theoretical approach that relies upon identification of the number of species present using electrophoretic methods, experimental measurement of ligand-metal charge transfer (LMCT) bands in the UV-Vis region, simulation of the UV-Vis spectra, and calculated thermodynamic quantities. The speciation of Rh(III) nitrate is shown to be straightforward; however, Rh(III) chloride speciation in acidic aqueous solutions is significantly more complex than prior work indicates.

III.b.1 Materials and Methods. Samples presumed to be $RhCl_3 \cdot nH_2O$ (99.99% Rh purity, Fisher) were dissolved in deionized distilled 18 MΩ water (D-DIW), under constant stirring at room temperature, except for daily low heating (1 h/day), until equilibrium was reached. Solutions were protected from light at all times. The Rh chloride speciation was perturbed by adding aliquots of $RhCl_3$ stock solutions, described above, to D-DIW and enough 12 M HCl (Fisher) to obtain various chloride concentrations (Table 1). The resulting solutions were stirred for 1 minute before being placed in a 50 °C oven, where they remained until solutions reached equilibrium. During this time, the solutions were stirred for 1 min daily and momentarily removed from the oven at recorded times for UV-Vis analysis (the solutions were allowed to cool down before measurements). Sodium (Na) concentrations in the $RhCl_3$ solutions in water were determined using an Atomic Absorption Flame Emission Spectrophotometer (Flame AA) (Shimadzu AA-6200) (Buck Scientific Na/K Hollow Cathode Lamp, lamp current 14V, slit width 0.2 nm, wavelength 589.0 nm). The instrument was calibrated with dilutions of a 1003 ppm Na standard solution in 5% HNO_3 (VHG Labs). Rhodium nitrate solutions were prepared in a similar fashion. A solid sample presumed to be $Rh(NO_3)_3 \cdot nH_2O$ (36% Rh metal basis by weight, Sigma-Aldrich) was dissolved in D-DIW. Once dissolved, the Rh nitrate solution turned yellow. An attempt was made to prepare $[Rh(NO_3)_x]$ (with $x > 3$), by adding aliquots of $[Rh(NO_3)_3]$ to D-DIW and concentrated HNO_3 (Fisher). Rh chloride and Rh nitrate samples reached equilibrium when UV-Vis spectra remained unchanged between two consecutive daily measurements.

UV-Vis spectra of the Rh chloride and Rh nitrate solutions were obtained at regular time intervals (at least weekly) using a Cary 5000 UV-visible spectrophotometer (Varian/Agilent). Solution absorbances were measured between 300 nm and 800 nm for the low-energy

absorption feature, and between 190 nm and 600 nm for the high-energy band. Rh samples were equilibrated with Rh concentrations of ca. 10^{-3} M, but subsequent UV-Vis measurements required dilutions. Low-energy UV-Vis measurements (λ = 300 – 800 nm) were performed with Rh concentrations at ca. 10^{-3}, while high-energy absorbance (λ = 190 – 600 nm) required Rh concentrations of ca. 10^{-5} M (Table 1). Rh concentrations were determined by Inductively Coupled Plasma Optical Emission Spectrometry (ICP-OES, Perkin Elmer Optima 3200 RL). The instrument was calibrated using dilutions of a 1000 ppm Rh standard solution in 10% HCl (Acros Organic).

Table 1. Concentrations of Rh (in M) used for data collection (after dilution) of the UV-Vis spectrum as a function of acid concentration employed during equilibration after addition of HCl or HNO_3.

Acid Concentration During Equilibration	Rh(M) during $\lambda_{UV\text{-}Vis}$ (190 – 600 nm)	Rh(M) during $\lambda_{UV\text{-}Vis}$ (300 – 800 nm)
0.0	9.2 (± 0.1)·10^{-6} (HCl)	9.2 (± 0.1)·10^{-4} (HCl)
	2.69 (± 0.06)·10^{-5} (HNO_3)	
0.1	1.09 (± 0.03)·10^{-5} (HCl)	1.09 (± 0.03)·10^{-3} (HCl)
0.5	1.05 (± 0.02)·10^{-5} (HCl)	1.05 (± 0.02)·10^{-3} (HCl)
1.0	1.03 (± 0.06)·10^{-5} (HCl)	1.03 (± 0.06)·10^{-3} (HCl)
2.0	9.9 (± 0.3)·10^{-6} (HCl)	9.9 (± 0.3)·10^{-4} (HCl)
	5.36 (± 0.05)·10^{-5} (HNO_3)	
4.0	2.73 (± 0.06)·10^{-5} (HNO_3)	
6.0	9 (± 1)·10^{-6} (HCl)	9 (± 1)·10^{-4} (HCl)
	2.73 (± 0.05)·10^{-5} (HNO_3)	
8.0	9.4 (± 0.6)·10^{-6} (HCl)	9.4 (± 0.6)·10^{-4} (HCl)
	5.36 (± 0.07)·10^{-5} (HNO_3)	
9.0	1.1 (± 0.1)·10^{-5} (HCl)	1.1 (± 0.1)·10^{-3} (HCl)
10.0	5.22 (± 0.05)·10^{-5} (HNO_3)	
12.0	2.99 (± 0.05)·10^{-5} (HNO_3)	

Capillary zone electrophoresis (CZE) (Agilent 7100 Capillary Electrophoresis System) was performed using the Rh solutions described in Table 1 to determine the minimum number of chloridated species and to estimate species charge. The observed number of species from CZE is considered the minimum number because the molar absorptivity for each of the Rh chlorides is quite small and may not be detectable at the concentrations employed. The capillary

(PolyMicro Technologies) was 60 cm long (53 cm to the detection window), with an inner diameter of 75 μm. The applied voltage spanned -30 and 30 kV to enable identification of both negative and positive species. The temperature of the capillary was held constant at 25 °C. Solutions were injected hydrodynamically at 5 mbar for 10 sec. UV-Vis (200 - 600 nm) was used for detection, in 2.0 nm increments. New capillaries were conditioned by flushing with 1.0 M KOH (5 min), D-DIW (5 min), 1.0 M HCl (5 min), D-DIW (5 min), and background electrolyte (BGE) (5 min). The preconditioning of the capillary consisted of flushing with 0.1 M KOH (5 min), D-DIW (5 min), 1.0 M HCl (5 min), D-DIW (5 min), and BGE (5 min). After the final run, post conditioning of the capillary consisted of flushing with D-DIW for 20 min. The background electrolytes that were used contained 10 mM $NaClO_4$, and various concentrations of HCl to match the concentration of the HCl of the different samples (Table 1). The pH of the BGE was adjusted to 3.7 with $HClO_4$. Acetone (1 M) was also added in some cases to identify the electroosmotic flow (EOF) band. Once the EOF was identified, the samples were run again in the absence of acetone to identify the absorption associated with Rh-containing species. Acetone that was added to some of the samples was detected at a wavelength of 280 nm and also with a contactless conductivity detector (TraceDec Contactless Conductivity Detector). OpenLAB CDS ChemStation (Agilent Technologies) was used for data analysis.

III.b.2 Computational Methods. The B3LYP combination of density functionals was employed for the optimization of the gas-phase hydrated Rh(III) as $[Rh(H_2O)_6]^{3+}$ and the chloride and nitrate substituted species $[RhCl_x(H_2O)_y^{3-x}]$ (x = 0 – 6; y = 6 – x), $[Rh(NO_3)_x(H_2O)_y^{3-x}]$ (x = 0 – 3; y = 6 – 2x) and $[Rh_2Cl_9^{3-}]$ using the NWChem software package. The cc-pVDZ basis set was used to describe all atoms. In the case of Rh(III), this consists of segmented contracted 4s4p3d1f functions, along with a matching pseudopotential that replaces the 28 inner-shell ($[Ar]4s^23d^8$) electrons. Frequency calculations were performed on all optimized structures to obtain thermochemical corrections and ensure they correspond to a local minima.

Single point conductor polarized continuum model (CPCM) calculations were performed as implemented in the development version of Gaussian09. The solvent corrected free energies (in water) of the replacement reactions that produce the chloride and nitrate species from the hydrated ion are defined by:

$$\Delta G_{rxn} = \Delta G_{gas}^{298} + \Delta G_{solv} + SS_{corr}$$

which has ΔG_{gas}^{298} as the free energy of the reaction in the gas-phase, ΔG_{solv} as the solvation contribution to the free energy of the reaction, and SS_{corr} as the standard-state thermodynamic correction (-4.3 kcal/mol for each $(H_2O)_n$ water cluster). Geometry optimization of $[RhCl_3(H_2O)_3]$ was performed in the solution phase using CPCM as a test to ensure a similar geometry and electronic structure was obtained. Indeed, the solution phase geometry exhibited only minimal elongation (< 0.1 Å) of the Rh-Cl and Rh-OH_2 bond lengths relative to the gas-phase.

As multiple species may exist experimentally, the goal of this work is to utilize the computed oscillator strengths for the electronic transitions to simulate the experimental UV-Vis spectrum in aqueous solution. A computational protocol that is easily adopted by a broader community is desired so as to maximize the general applicability of a combined experimental and computational approach to dissect the complex speciation of metal ions in solution. As

such, Time-Dependent DFT (TD-DFT) was used to compute the excited state energies and transition oscillator strengths in solution for each optimized Rh(III) species. It is, however, quite difficult for a single density functional to optimally describe all of the different types of excited states in a transition metal complex simultaneously (charge transfer vs. *d-d* transitions, for example). Thus, we have focused upon accurate reproduction of the high energy ligand-to-metal charge-transfer based electronic transitions for Rh complexes using the long range corrected PBE0 (LC-wPBE) functional, which has exhibited much success in predicting these types of excitations. The basis sets for the TD-DFT calculations utilized the aug-cc-pVTZ with the corresponding pseudopotential for Rh (III) and aug-cc-pVTZ basis sets for all other atoms. Larger basis sets were used in the TD-DFT calculations as opposed to geometry optimizations, as a more complete basis set yields better orbital descriptions. Several different continuum models (CPCM, IEF-PCM, and COSMO) were examined for the accurate reproduction of the UV-Vis spectrum of a single species, $[Rh(NO_3)_3]$, with only CPCM being successful (*vide infra*).

To compare theoretical data with experiment, oscillator strengths for the electronic transitions calculated in Gaussian09 were converted to molar absorptivity using:

$$\varepsilon_i(\tilde{\nu}) = \frac{e^2 N\sqrt{\pi}}{1000\ln(10)c^2 m_e}\frac{f_i}{\sigma}\exp\left[-\left(\frac{\tilde{\nu}-\tilde{\nu}_i}{\sigma}\right)^2\right]$$

where ε_i is the electronic excitation of interest, e = 4.803204x10^{-10} esu, N = 6.02214199x10^{23}, c = 2.997924x10^{10} cm/s, m_e = 9.10938x10^{-31} g, f_i is the oscillator strength, σ = 0.5 eV which is the standard deviation in wavenumbers and is related to the width of the band, and at the maximum of the band where the energy of the incident radiation, $\tilde{\nu}$, is equal to $\tilde{\nu}_i$.[30] When there are multiple electronic excitations in the spectral region of interest, the spectrum becomes a sum of all of the individual bands:

$$\varepsilon(\tilde{\nu}) = \sum_{i=1}^{n} \varepsilon_i(\tilde{\nu})$$

The resulting theoretical spectra were then used to fit the experimental spectrum based upon the relative concentrations of different Rh(III) species by minimizing the normalized root mean squared deviation (NRMSD) between the combined theoretical spectrum and the experimental one through modification of the percent contribution of each Rh(III) chloride species. This is directly analogous to deconvoluting the experimental spectrum into sub-species experimental spectra. A NRMSD of 5% was chosen as a threshold for a fit to be considered reasonable, and the combinations that yielded a NRMSD below the threshold were examined.

III.b.3 Results and Discussion

Prior to this work, the speciation of Rh in nitric acid had not been extensively studied, but is believed to be heavily influenced on the initial Rh complex dissolved in solution. X-ray diffraction studies performed by Belyaev et. al. and Caminiti et. al. suggest the presence of a Rh (III) dimer in acidic solutions where the $[NO_3^-]$ > 1 M and Rh concentrations of 10^{-1} M. At lower Rh(III) concentrations, like those present in SNF, a monomeric Rh (III) nitrate species was suggested, which has been supported by UV-Vis and capillary electrophoresis data obtained in acidic media by Aleksenko et. al.

Here, the speciation of Rh(III) in nitric acid was first examined by calculating the thermodynamic favorability of successive nitrate additions to an initial $[Rh(H_2O)_6]^{3+}$ cluster in aqueous solution (Table 2). Initial geometries presumed a bidentate coordination geometry for the nitrate, as observed previously with other transition metal nitrate complexes. Stable monodentate bound nitrates were pursued but no low-energy optimized structures were found, nor were any species that contained four or more nitrates in the primary coordination sphere. The optimized structures exhibited an increase in the bond length $r_{Rh\text{-}O_2NO}$ and $r_{Rh\text{-}OH_2}$ with each subsequent nitrate replacement. Beginning with the octahedral hydrated ion, each nitrate addition is very thermodynamically favorable ($\Delta G_{rxn} \leq$ -44 kcal/mol), indicating that the trinitrate complex is likely to be present in aqueous solution (Table 2) and that bound nitrates are unlikely to dissociate until a stronger complexant is added to solution. The theoretical spectra of the aqueous mono-, di-, and tri-nitrate species of Rh(III) are predicted to have distinct peak positions between 184 to 202 nm in the UV-Vis spectrum. These absorption bands are found to derive from LMCT transitions. Based upon these calculations, different nitrate species should be clearly evident within the experimental UV-Vis spectrum.

Table 2. Calculated solution-phase free energies of the successive nitrate addition reactions to the initial $[Rh(H_2O)_6]^{3+}$ species (in kcal/mol), along with the TD-DFT calculated λ_{max} (in nm) of the $Rh(NO_3)_x(H_2O)_y^{3-x}$ (x = 0 – 3; y = 6 – 2x) products between 180 and 800 nm.

Rxn	ΔG_{rxn}	λ_{max}(product)
$[Rh(H_2O)_6]^{3+}_{(aq)} + NO_3^-_{(aq)} \rightarrow [Rh(H_2O)_4(NO_3)]^{2+}_{(aq)} + 2H_2O_{(aq)}$	-44.55	184
$[Rh(H_2O)_4(NO_3)]^{2+}_{(aq)} + NO_3^-_{(aq)} \rightarrow [Rh(H_2O)_2(NO_3)_2]^{+}_{(aq)} + 2H_2O_{(aq)}$	-15.73	196
$[Rh(H_2O)_2(NO_3)_2]^{+}_{(aq)} + NO_3^-_{(aq)} \rightarrow [Rh(NO_3)_3]_{(aq)} + 2H_2O_{(aq)}$	-13.05	202

The experimental data reinforces the thermodynamic predictions of a single species of Rh(III), $[Rh(NO_3)_3]$, in nitrate media. The stock solution of 10^{-3} Rh(III) nitrate reached equilibrium after three weeks of continuous stirring, during which the solution color changed from clear to yellow. A UV-vis spectrum was obtained in the 800 – 300 nm range to examine the low-energy transitions, where *d-d* transitions are typically manifested. No distinct peaks were observed, indicating high symmetry structures with forbidden *d-d* transitions. A peak below 300 nm with a molar absorptivity much larger than 1000 was observed, having a peak position of 202 nm. The samples of the stock solutions with nitrate concentration between 0 and 12 M, presented in Table 1, were continuously stirred and reached equilibrium in a week. UV-Vis spectra exhibit one absorbance band in all solutions with a λ_{max} = 202 nm (molar absorptivies were within error of each other and had a value of 22,310 $M^{-1}\cdot cm^{-1}$). Examination of the theoretical spectrum of $[Rh(NO_3)_3]$ using a 0.5 eV Gaussian bandwidth reveal a single peak deriving from LMCT transitions also centered at 202 nm. As shown in Figure 2, the $[Rh(NO_3)_3]$ theoretical spectrum

has only a 3% NRMSD with the experimental spectrum of $[Rh(NO_3)_3]$ dissolved in water, with the position of the band at 202 nm, the band shape, and its absorptivity, being accurately reproduced. In combination, the theoretical and experimental data indicate that the presumed $[Rh(NO_3)_3]$ that was initially dissolved in solution is maintained in the molecular form in the aqueous phase and at varying concentration of nitric acid. Based upon calculated thermodynamic data, it is further anticipated that in other solution-phase environments where 10^{-3} M Rh(III) is dissolved in nitric acid, once the $[Rh(NO_3)_3]$ is formed it will be the stable kinetic and thermodynamic end product in the absence of another strong complexant. The significantly different λ_{max} values predicted for each of the $[Rh(H_2O)_4(NO_3)]^{2+}$, $[Rh(H_2O)_2(NO_3)_2]^{+}$, and $[Rh(NO_3)_3]$ species should help in species identification in future studies.

Figure 2. Experimental spectrum of $[Rh(NO_3)_3]$ ([Rh] ca. 10^{-5}M) dissolved in pure water (blue) overlayed with the LC-wPBE/aug-cc-pVTZ (red) predicted UV-Vis spectrum with the primary orbitals involved in the dominant transition shown.

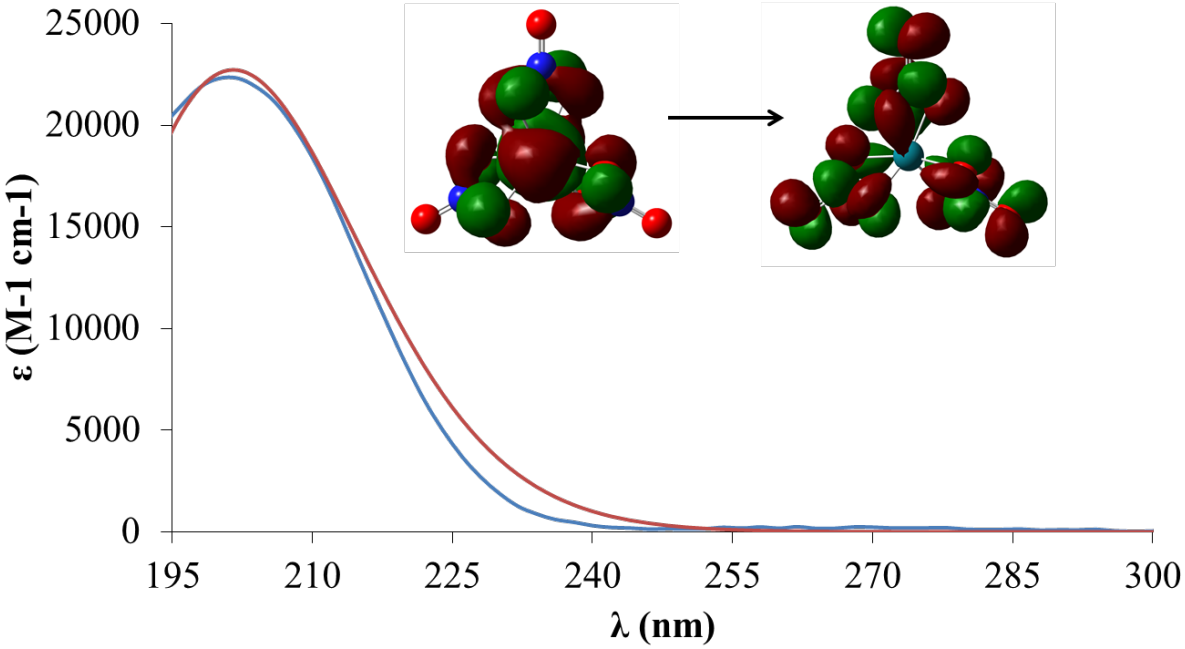

Past studies have demonstrated that speciation of Rh(III) in hydrochloric acid is complex. Species identification has relied heavily on UV-Vis spectroscopy, focusing on the absorptions between 300 and 800 nm (presumably the *d-d* absorption bands which have a limited allowedness due to low symmetry). After separation using chromatography, a study of Wolsey et. al. determined the identifying UV-Vis peak positions and molar absorptivities in this range for all of the chloridated Rh(III) aqua species in solution conditions that spanned 0.1 M to 2 M HCl. Subsequent studies focused on the chloride exchange reactions in the first coordination sphere. These works have suggested that successive chloride substitution reactions of $[Rh(H_2O)_6]^{3+}$ to form $[RhCl_5(H_2O)]^{2-}$ are favorable in solution where the concentration of HCl is greater than 0.07 M. The formation of $[RhCl_6]^{3-}$ is unfavorable and is only possible at temperatures above 70 °C, as would be expected based upon the relative steric bulk of the chloride ligands, the ionic radius and electrophilicity of Rh(III). Most of these studies have been performed at temperatures greater than or equal to 50 °C and in the presence of perchloric acid. Thus the reported thermodynamic favorability of chloride substitution may be

diminished under the room temperature conditions anticipated for SNF raffinates. Importantly, the complex species distribution of Rh(III) in HCl solution has not been systematically pursued. Aleksenko et. al. studied Rh(III) speciation under the two extremes of 0.1 M and 11 M HCl using capillary electrophoresis to separate the species in solution, with a subsequent report of the UV-Vis spectra of LMCT bands for identification of the individual species. In general, as the concentration of HCl was increased, the number of chlorides coordinated to Rh(III) increased, and a mixture of Rh chloride species was suggested at both chloride concentrations. However, Aleksenko's reported UV-Vis λ_{max} = 250 nm differs from other reports that established a stepwise shift to shorter wavelengths of all the absorbance bands upon substitution of H_2O for Cl^- ligands, suggesting the presence of a complex mixture in solution. Thus, disparity exists regarding both profile the higher energy absorbance bands in the UV-Vis spectra of individual Rh(III) chloridated species and the speciation of Rh(III) as the concentration of hydrochloric acid is increased. The results and discussion herein first describe the overall features of the TD-DFT predicted spectra of Rh(III) chloride species as the number of chloride ligands is increased, and experimental UV-Vis spectra as the concentration of HCl is increased. Then the speciation of dissolved Rh(III) chloride is established using data from the predicted thermodynamic properties of chloride substitution, the TD-DFT spectra, along with capillary zone electrophoresis data.

The TD-DFT UV-Vis absorption spectra of $[RhCl_x(H_2O)_y]^{3-x}$ (x = 0 – 6; y = 6 – x) contain one to two distinct absorption peaks below 300 nm for each species, with a general red shift upon the each chloride substitution. It is important to note that there are distinct differences in the predicted spectra of Rh(III) chloride species depending upon the isomer. In the case of the *cis*- and *trans*- $[RhCl_2(H_2O)_4]^+$ and $[RhCl_4(H_2O)_2]^-$, individual species have λ_{max} differing by ≥ 10 nm. This is relevant as prior separations and identification of the high energy region of the UV-Vis spectra have not distinguished contributions from different isomeric species that may be present. When considering the spectra obtained from Rh(III) in a wide range of chloride concentrations, unique absorption bands are observed; however, the peak positions and shapes do not agree with the predicted spectra for a single species (Figure Sxx) nor the prior reported peak positions reported by Blasius or Aleksenko for isolated Rh(III) chloride species. The experimental spectra do exhibit the anticipated red-shift in the 300 - 800 nm absorbance peaks, consistent with an overall increase in chloride coordination with increased HCl (Table 3).

Table 3. Literature UV-Vis λ_{max} (in nm) for individual Rh species and UV-Vis absorption maxima as a function of the HCl concentration of the Rh chloride solutions. References are provided in *Inorganic Chemistry* ***2014*** *53, 12315-12322*

Species	λ_1	λ_2	Reference	λ_3	λ_4	Reference
$[RhCl(H_2O)_5]^{2+}$				335	426	[34]
cis-$[RhCl_2(H_2O)_4]^+$	201	220	[35]	355	450	[14]
trans-$[RhCl_2(H_2O)_4]^+$				350	450	[14]
cis-$[RhCl_3(H_2O)_3]$	201	223	[35]	376	474	[34]
trans-$[RhCl_3(H_2O)_3]$				370	471	[34]
$[RhCl_4(H_2O)_2]^-$	201	223	[35]	385	488	[34]
$[RhCl_5(H_2O)]^{2-}$	201	242	[35]	402	507	[34]
$[RhCl_6]^{3-}$	207	253	[35]	411	518	[34]
$[Rh_2Cl_9]^{3-}$				414	524	[8]

HCl (M)	λ_1	λ_2	λ_3	Reference
0.0	221	357	449	Present work
0.1	225	368	465	Present work
0.5	225	374	471	Present work
1.0	226	385	484	Present work
2.0	226	396	497	Present work
6.0	249	410	511	Present work
9.0	250	408	517	Present work

The dissolution of the Rh chloride sample in D-DIW occurred within minutes, while several months were necessary to reach a meta-stable solution equilibrium defined by unchanging UV-Vis spectra over the course of several days. This is important, as prior work has suggested that the solution composition can change for Rh(III) in HCl over the course of years. During the dissolution and equilibrium process the solution color changed from red to yellow. The high-energy feature of the UV-Vis spectrum for the 0 M HCl solution has a maximum at 221 nm, while the lower energy portion of the spectrum contains two features with maxima at 369 nm and 463 nm, respectively (Table 3). Prior assignment of the low-energy absorptions of the isolated meridional isomer of aqueous $[RhCl_3(H_2O)_3]$ have wavelength maxima of 471 nm and 370 nm, while the facial isomer has maxima at 474 nm and 376 nm.

Based upon these literature data, it is apparent that a mixture of species results from dissolution of the initial sample, as the peak at 463 nm cannot arise from either the *facial* or *meridional* isomers (λ_{max} of 474 nm and 471 nm, respectively), or any mixture of these two species. The reported *d-d* absorbance bands of isolated *cis*-$[RhCl_2(H_2O)_4]^+$ are located at 358 nm and 453 nm, while that of $[RhCl(H_2O)_5]^{2+}$ occur at 335 nm and 426 nm (Table 3). Thus, it is

likely that some of these mono- and dichlorido species exist in solution and are responsible for the deviations in the *d-d* band positions. The possibility of the Rh(III) chloride sample having impurities that may result in multiple species in the aqueous solution is confirmed by Flame AA analysis, which indicates a small $3 \cdot 10^{-3}$ Na-to-Rh mole ratio in the solution of the dissolved sample prepared in D-DIW. Consequently, it is envisioned that Na^+ was introduced in the sample as counterion to chloride and the $RhCl_3 \cdot nH_2O$ sample maybe a mixture of $[RhCl_x(H_2O)_{x-6}]^{3-x}$ species that derive from the methodology for preparation.[36] The capillary electrophoresis data indicates the presence of a neutral species in solution; however, this value is used as a lower bound to the potential number of species present because the CZE may omit the presence of some species due to the low molar absorptivities at the concentration employed and may not resolve isomers. A linear combination of the TD-DFT spectra of the *facial* and *meridional* isomers of $[RhCl_3(H_2O)_3]$ yields a fit to the LMCT portion of the experimental UV-Vis spectrum having an NRMSD of 6%, beyond the threshold of acceptable tolerance for fitting. NRSMD values below 5% are obtained when the relative composition of the spectrum is 0 – 6% *trans*-$[RhCl_2(H_2O)_4]^+$, 48 – 50% *cis*-$[RhCl_2(H_2O)_4]^+$, and 46 – 50% *mer*-$[RhCl_3(H_2O)_3]$ (Figure 3). The very best NRMSD value of 3% is obtained with 3% *trans*-$[RhCl_2(H_2O)_4]^+$, 49% *cis*-$[RhCl_2(H_2O)_4]^+$ and 48% *mer*-$[RhCl_3(H_2O)_3]$. Note that the NRMSD values are only calculated above 210 nm, as the absorption intensity in the UV-Vis spectrum below 210 nm is due to excess aqueous chloride, which has a λ_{max} of 193 nm and has not been modeled in the TD-DFT simulations.[37] From a thermodynamic perspective, prior work and the calculated free energies for chloride substitution determined here indicate a strong driving force for chloride substitution (Table 4). However, in pure water there is little excess chloride and thus it is believed that the speciation in the 0 M HCl solution is unchanged relative to the original sample.

Figure 3. Experimental spectrum of the Rh(III) chloride sample dissolved in pure water (blue) overlayed with the LC-wPBE/aug-cc-pVTZ (red) predicted UV-Vis spectrum that results from fitting the individual absorption contributions of all optimized Rh chloride species. The relative concentration ranges span all fits whose NRMSD values were below a tolerance threshold of 5% relative to experiment. The optimized structures of the major species along with their key bond lengths are presented.

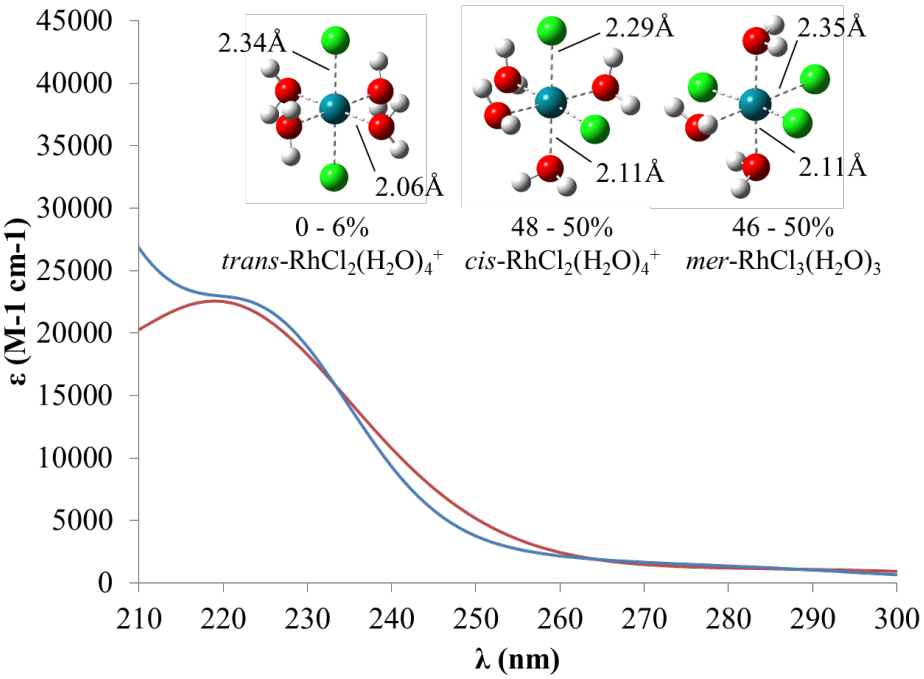

As reported in Table 4, addition of chloride to the di- and trichlorido species believed to be present in upon dissolution of the sample should be exergonic until formation of the hexachlorido species. This agrees qualitatively with the experimental free energies of reaction obtained from kinetic studies performed at elevated temperatures. The theoretical values at 298K are 5 – 10 kcal/mol higher thatn that obtained between 303 – 318 K. As chloride is added, the ΔG_{rxn} becomes systematically less favorable, with formation of the $[RhCl_5(H_2O)]^{2-}$ species from $[RhCl_4(H_2O)_2]^-$ having a free energy of only ca. -5 kcal/mol. Therefore, we expect that the highly chloridated species should form only at high chloride concentration. Under the equilibration conditions, oligomers of Rh chloride can also be produced and thus the competitive reactions of the various chloridated species to form the dimer $[Rh_2Cl_9]^{3-}$ were also investigated. As seen in Table 5, the addition of chloride to $[RhCl_3(H_2O)_3]$ is thermodynamically favored with a ΔG_{rxn} of -13.5 kcal/mol; however, a secondary pathway that is also favored is the bimolecular reaction of $[RhCl_3(H_2O)_3]$ with itself to form $[Rh_2Cl_9]^{3-}$, having ΔG_{rxn} of -4.5 kcal/mol. Given that we do not know the activation barriers for these processes, it is possible that $[Rh_2Cl_9]^{3-}$ could accumulate over time and be present in solution with the various monomeric chloridated Rh species. As the chloride solutions were equilibrated with millimolar concentrations of Rh(III), the formation of polymeric species solution is not

unreasonable, however we note that preparation of these species often employs large stabilizing ligands (e.g. triethyl phosphine) in the remainder of the coordination sphere of Rh(III). The formation of $[Rh_2Cl_9]^{3-}$ is also predicted from reaction of $[RhCl_6]^{3-}$ with $[RhCl_3(H_2O)_3]$; however, this pathway is less likely in solution, as it would require significant concentrations of both the hexa- and trichlorido- species, and the DFT results indicate that formation of the hexachlorido complex is thermodynamically unfavorable. Thus, based upon the thermodynamic analysis of the different chloride addition and bimolecular reactions outlined in Table 4, DFT predicts that as chloride concentration increases, more substituted chloride species, should form with the potential for dimeric $[Rh_2Cl_9]^{3-}$ being present after the formation of the trichlorido complex $[RhCl_3(H_2O)_3]$.

Table 4. Solution-phase B3LYP/cc-pVDZ predicted ΔG_{rxn} (kcal/mol) of chloride complexation reactions in aqueous solution.

Chemical Reaction	ΔG_{rxn}
$[Rh(H_2O)_6]^{3+} + Cl^- \rightarrow RhCl(H_2O)_5]^{2+} + H_2O$	-32.9
$[RhCl(H_2O)_5]^{2+} + Cl^- \rightarrow$ *cis*-$[RhCl_2(H_2O)_4]^+ + H_2O$	-4.2
$[RhCl(H_2O)_5]^{2+} + Cl^- \rightarrow$ *trans*-$[RhCl_2(H_2O)_4]^+ + H_2O$	-2.2
cis-$[RhCl_2(H_2O)_4]^+ + Cl^- \rightarrow$ *fac*-$[RhCl_3(H_2O)_3] + H_2O$	-13.1
trans-$[RhCl_2(H_2O)_4]^+ + Cl^- \rightarrow$ *fac*-$[RhCl_3(H_2O)_3] + H_2O$	-14.0
cis-$[RhCl_2(H_2O)_4]^+ + Cl^- \rightarrow$ *mer*-$[RhCl_3(H_2O)_3] + H_2O$	-12.6
trans-$[RhCl_2(H_2O)_4]^+ + Cl^- \rightarrow$ *mer*-$[RhCl_3(H_2O)_3] + H_2O$	-13.5
fac-$[RhCl_3(H_2O)_3] + Cl^- \rightarrow$ *cis*-$[RhCl_4(H_2O)_2]^- + H_2O$	-7.4
fac-$[RhCl_3(H_2O)_3] + Cl^- \rightarrow$ *trans*-$[RhCl_4(H_2O)_2]^- + H_2O$	-6.2
mer-$[RhCl_3(H_2O)_3] + Cl^- \rightarrow$ *cis*-$[RhCl_4(H_2O)_2]^- + H_2O$	-7.9
mer-$[RhCl_3(H_2O)_3] + Cl^- \rightarrow$ *trans*-$[RhCl_4(H_2O)_2]^- + H_2O$	-6.7
cis-$[RhCl_4(H_2O)_2]^- + Cl^- \rightarrow [RhCl_5(H_2O)]^{2-} + H_2O$	-4.8
trans-$[RhCl_4(H_2O)_2]^- + Cl^- \rightarrow [RhCl_5(H_2O)\ ]^{2-} + H_2O$	-6.0
$[RhCl_5(H_2O)]^{2-} + Cl^- \rightarrow [RhCl_6]^{3-} + H_2O$	1.9
$[RhCl_3(H_2O)_3] + [RhCl_3(H_2O)_3] + 3Cl^- \rightarrow [Rh_2Cl_9]^{3-} + 6H_2O$	-4.5
$[RhCl_3(H_2O)_3] + [RhCl_4(H_2O)_2]^- + 2Cl^- \rightarrow [Rh_2Cl_9]^{3-} + 5H_2O$	0.8
$[RhCl_4(H_2O)_2]^- + [RhCl_4(H_2O)_2]^- + Cl^- \rightarrow [Rh_2Cl_9]^{3-} + 4H_2O$	6.0
$[RhCl_4(H_2O)_2]^- + [RhCl_5(H_2O)]^{2-} \rightarrow [Rh_2Cl_9]^{3-} + 3H_2O$	6.5
$[RhCl_5(H_2O)]^{2-} + [RhCl_3(H_2O)_3] + Cl^- \rightarrow [Rh_2Cl_9]^{3-} + 4H_2O$	1.2
$[RhCl_3(H_2O)_3] + [RhCl_6]^{3-} \rightarrow [Rh_2Cl_9]^{3-} + 3H_2O$	-0.7

Table 5. Calculated speciation of Rh(III) complexes in various concentrations of HCl with relative concentrations that provide a NRMSD ≤ 5%. For HCl concentrations above 2 M a fit with a NRMSD ≤ 5% was not found.

Rh(III) Species	0 M	0.1 M	0.5 M	1.0 M	2.0 M
cis-$[RhCl_2(H_2O)_4]^+$	48 - 50%	0%	0%	0%	0%
trans-$[RhCl_2(H_2O)_4]^+$	0 - 6%	46 - 50%	40 - 48%	0%	0%
fac-$[RhCl_3(H_2O)_3]$	0%	0%	32 - 34%	56 - 60%	0%
mer-$[RhCl_3(H_2O)_3]$	46 - 50%	50 - 54%	20 - 26%	34 - 36%	0%
cis-$[RhCl_4(H_2O)_2]^-$	0%	0%	0%	1 - 3%	78 - 86%
$[RhCl_5(H_2O)]^-$	0%	0%	0%	0%	0%
$[RhCl_6]^{3-}$	0%	0%	0%	0%	0%
$[Rh_2Cl_9]^{3-}$	0%	0%	0%	4 - 6%	14 - 22%

Using the calculated UV-Vis absorption spectra of individual $[RhCl_x(H_2O)_{6-x}]^{3-x}$, the experimental spectra were fit to determine the relative concentrations of every complex under different HCl concentrations. As seen in Figure 4, the width of the LMCT peak broadens even at an HCl concentration of 0.1 M, indicating a change in the speciation that is described by the linear combination of TD-DFT excitations of both $[RhCl_2(H_2O)_4]^+$ and $[RhCl_3(H_2O)_3]$ species (Table 5). The TD-DFT spectra with an NRMSD ≤ 5% have relative concentrations of *trans*-$[RhCl_2(H_2O)_4]^+$ of 46 – 50% and *mer*-$[RhCl_3(H_2O)_3]$ of 50 – 54%. This is also supported by CZE data, as a neutral species is observed. It is interesting to note that in the added HCl medium the trans isomer of $RhCl_2(H_2O)_4]^+$ predominates, while the cis was prevalent in the original dissolution of the sample in pure water. While we do not have a ready explanation for this observation, we observe only a minimal energy difference between the two isomers, with the cis form being preferred for formation from the $RhCl(H_2O)_5^{2+}$ species. However, the calculated computed free energies for chloride addition are somewhat larger than observed experimentally (albeit at higher temperatures). Thus, it is possible that the complex equilibria that results when excess chloride is present will involve not only the chloride addition reactions, but also some extent of dissociation reactions of the trichloride species which favor the trans isomer. Increasing the concentration to 0.5 M reveals further broadening of the absorption band and a 1 nm shift in the peak position. The best fit to experiment results from a mixture of the absorption spectra of *trans*-$[RhCl_2(H_2O)]_4$ (40 – 48%), *fac*-$[RhCl_3(H_2O)_3]$ (32 – 34%), and *mer*-$[RhCl_3(H_2O)_3]$ (20 – 26%). Data from CZE data indicates the presence of at least the neutral species in 0.5 M HCl. The dominant species in 1.0 M HCl is predicted to be the $[RhCl_3(H_2O)_3]$ with a small concentrations of $[RhCl_4(H_2O)_2]^-$ and $[Rh_2Cl_9]^{3-}$. Two species are observed in 1.0 M HCl solution based on the CZE data, one neutral and the other negatively charged.

Determination of the speciation in solution using TD-DFT becomes difficult as the concentration of chloride reaches 2 M. The NRMSD for each fit is ~ 10% for each sample above 2 M HCl which suggests that either a more complex solution is formed

that contains an unknown species, or that the change in the bulk solution properties (ionic strength and dielectric constant) begin to alter the experimental spectrum. When the chloride concentration reaches 6 M the fitted TD-DFT spectrum would indicate that the absorbance associated with $[Rh_2Cl_9]^{3-}$ begin to dominate the spectrum, which reproduces the experimental observation that the entire high-energy band is red-shifted to a value between 250 and 260 nm. Data from CZE for the solutions for 2 M HCl and above all indicate the presence of two distinct species in solution with charges of -2 and -3. This agrees well with predicted speciation determined through TD-DFT fitting in that only two species are seen to dominate in solution where the concentration of HCl is ≥ 2 M. It is important to note that the hexa-chlorido complex is not seen in the range of 0 to 12 M HCl. This is also consistent with the calculated thermodynamic data from both literature and the calculated thermodynamic data presented in this work.

Figure 4. Experimental spectrum of the dissolved Rh chloride sample in (A) 0.1 M HCl, (B) 0.5 M HCl, and (C) 1.0 M HCl (blue) overlayed with the predicted LC-wPBE/aug-cc-pVTZ UV-Vis spectrum (red) that results from fitting the individual absorption contributions of all optimized Rh chlorido species. The relative concentration ranges span all fits whose NRMSD values were below a tolerance threshold of 5% relative to experiment.

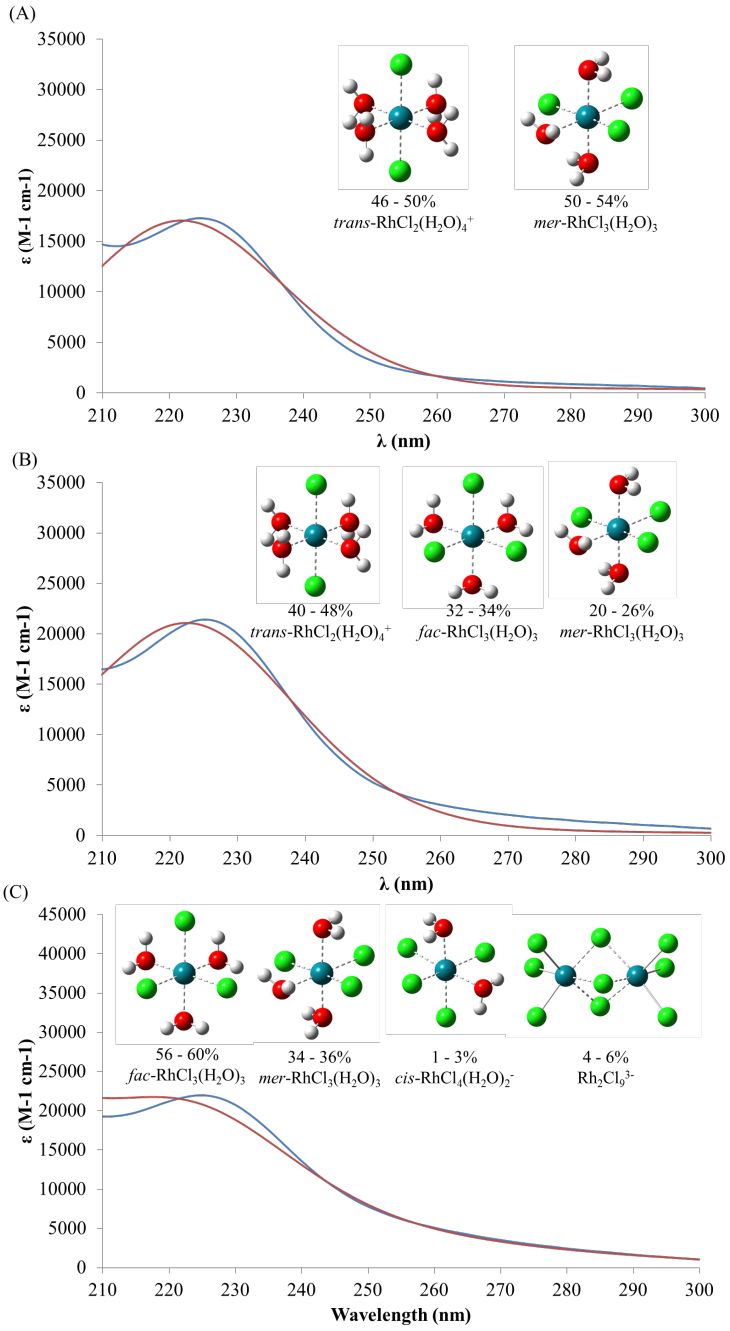

III.b.4 Conclusions

The speciation of Rh(III) in hydrochloric and nitric acid solutions has been investigated using experimental (UV-Vis, CZE) and theoretical (thermodynamic, TD-DFT) techniques. The evidence presented indicate that in HCl solutions, Rh(III) exists as a mixture of species specifically $[RhCl_x(H_2O)_y]^{3-x}$ (x = 0 – 6; y = 6 – x) and $[Rh_2Cl_9]^{3-}$. The $[RhCl_6]^{3-}$ species was not observed in this study, agreeing with data reported in the literature showing the substitution of the sixth chloride as non-spontaneous at room temperature. As the concentration of HCl increases, increased chloride coordination is observed with Rh(III) and an apparent red shift occurs for both the LMCT and *d-d* bands of the UV-Vis spectra. This trend is supported by the theoretical free energies of chloride addition and CZE data. In contrast, the speciation of Rh(III) in HNO_3 is invariant to the concentration of HNO_3. The UV-Vis spectra for Rh(III) in 0 - 12 M HNO_3 show a single peak with a λ_{max} of 202 nm; in agreement with the simulated TD-DFT spectrum of $[Rh(NO_3)_3]$. The complex speciation of Rh(III) in chloride medium relative to nitrate is likely due to a combination of factors, including smaller binding energies of chloride for substitution beyond $[RhCl_3(H_2O)_3]$ and a more divers coordination environment caused by the monodentate nature of chloride relative to the thermodynamically preferred bidentate coordination mode of nitrate. In combination, these data help to clarify and assess the speciation of Rh(III) in acidic media relevant to separations and purification of this precious metal from spent fuel raffinates. The utilization of modern computational methods in combination with experimental techniques also points to a general protocol that can be successfully pursued to determine speciation of precious metals in acidic media.

III.c Extraction of Rh(III) By Phosphinic Acids *(Solvent Extraction and Ion Exchange, **2015**, 33, 418-428)*

In order to understand the basic mechanisms and types of complexes formed during Rh(III) extraction, known ligands were first pursued so as to validate concepts that emerged from CADME. The solvent extraction of Rh(III) in chloride media has been established in the literature – although not necessarily in conditions relevant to SNF raffinates, with an emphasis upon separating Rh(III) from other PGMs. Independent studies by Zou et. al., and Mhaske and Dhadke have demonstrated that Rh(III) can be separated, and nearly completely extracted, under these conditions using commercially available extractants and tin. Alam et. al. explored the use of the extractant Kelex 100 (7-(4-ethyl-1-methyloctyl)-8-hydroxyquinoline) in which tin was not used, however Rh(III) extraction never exceeded 20%. A recent study by Lee et. al. has shown that Rh(III) can be extracted using the neutral extractant tri-iso-octylamine, with a maximum extraction of 36.3% in presence of 8 M chloride. Despite advances in the solvent extraction of Rh(III) in chloride media, few studies on the extraction of Rh(III) from nitrate media similar to SNF raffinates are present in the literature. Work by Patel and Thornback demonstrated that an acidic extractant can be used to target Rh(III), specifically dinonylnapthalene

sulphonic acid, with the addition of nitrite to the aqueous phase and at temperatures above 50 °C.

The aim of the current work is to test commercially available extractants for the ability to extract Rh(III) in nitrate media, conditions relevant to SNF raffinates. In particular, diphenylphosphinic acid (DPPA) and diphenyldithiophosphinic (DPDTPA) acid were tested. These extractants were chosen for their stability in contact with nitric acid and radiolytic stability. Phosphinic extractants have shown great success for the separation of actinides from lanthanides. One such extractant, Cyanex 301, demonstrated preferential binding to trivalent actinides over trivalent lanthanides. Though we primarily utilize experimental techniques in this work to determine extraction equilibrium constants with these organic acids, limited computational studies have been used to elucidate which terms may dominate the thermodynamics of the extraction process.

III.c.1 Experimental and Computational Methods

Solid $Rh(NO_3)_3 \cdot nH_2O$ (36% Rh metal basis by weight, Sigma-Aldrich) was dissolved in distilled deionized 18 MΩ water and prepared similar to previous work. Working Rh(III) solution concentrations were ca. 10^{-4} M. Speciation determined by earlier work indicates that the primary Rh(III) species in solution is $Rh(NO_3)_3$. Rh(III) concentrations were determined by Inductively Coupled Plasma Optical Emission Spectrometry (ICP-OES) (Perkin Elmer Optima 3200 RL). The instrument was calibrated with dilutions of a 1000 ppm Rh(III) standard solution in 10% HCl (Acros Organic).

DPPA (99%) was purchased from Acros Organics. The DPDTPA was obtained from Alfa Aesar. A suitable organic solvent that allowed for the dissolution of both DPPA and DPDTPA was not found. A $1.9 \cdot 10^{-2}$ M stock solution of DPPA was prepared in 1-pentanol (99%, Extra Pure, Acros Organics). The DPDTPA stock solution was prepared in toluene (99+%, Extra pure, Acros Organics) to be $1.89 \cdot 10^{-2}$ M. The stock solutions were continuously stirred for at least 24 hours before use. Extractant solutions were kept in the dark.

The influence of pH on the speciation of the $Rh(NO_3)_3$ stock aqueous solution was tested via solution absorbance measurement (Agilent Cary 5000 UV-visible spectrophotometer); the solution absorbance at 400 nm increases from 0.113 at pH 3 to 0.147 at pH 10, indicating a change of $Rh(NO_3)_3$ stock solution speciation modification with pH. For extraction experiments, equal volumes of aqueous solutions of Rh(III) nitrate and extractant solutions (Vaq = Vorg = 4 mL) were equilibrated in triplicate using a sample rotator (Glas-Col). Rh(III) concentrations in the original and final aqueous solutions were measured using Inductively Coupled Plasma Optical Emission Spectrometry (ICP-OES, Perkin Elmer Optima 3200 RL), and was calibrated with dilutions of a 1000 ppm Rh(III) standard solution in 10% HCl (Acros Organic). The Rh(III) concentration of sample organic phases were calculated by subtraction of original and final aqueous solution concentrations. To study the dependency of the extractant concentration, the sample pH was adjusted to 3.32 with diluted sodium hydroxide

solutions (certified ACS, Fisher) using a double junction Ag/AgCl reference accuTupH Rugged Bulb pH electrode (Fisher) and an Accumet Basic AB15 pH meter (Fisher). Sample pH values were checked and adjusted hourly until equilibration was reached. The samples were equilibrated until the pH remained unchanged between two hourly time intervals; it was assumed that the extraction had then reached equilibrium.

The extraction samples were allowed to equilibrate for an additional 16 hours on the rotator and the pH was checked again to ensure that the pH remained unchanged and that equilibrium was indeed reached. The nitrate ion concentration dependency was tested in a similar fashion as the extractant dependency work; the extractant concentration was fixed at $1.9 \cdot 10^{-2}$ and pH was fixed at 3.32; the nitrate ion concentration was varied from $1.0 \cdot 10^{-3}$ M to 1 M. To study the pH dependency, HCl (Certified ACS Plus, Fisher) was used to vary the pH. It is important to ensure that Rh(III) speciation was not affected by the presence of chloride, as prior work has indicated the ability of chloride to undergo substitution with nitrate ions coordinated to Rh(III). It was determined that a contact time of 8 hours was sufficient to reach extraction equilibrium with both extractants when the pH was not fixed. Additionally, $Rh(NO_3)_3$ solution speciation stability with time was tested via solution absorbance measurements at 400 nm (Agilent Cary 5000 UV-visible spectrophotometer); a noticeable decrease of the Rh(III) solution absorbance was found 12 hours after addition of HCl, which demonstrates that HCl does not affect $Rh(NO_3)_3$ solution speciation within the 8 hours of equilibration necessary for complete extraction. Extraction experiments were performed with hydrogen ion concentrations that varied from $3.0 \cdot 10^{-4}$ M to 1.0 M in the pH dependent extractions while the extractant and nitrate ion concentration were held constant at $1.9 \cdot 10^{-2}$ M and $1.0 \cdot 10^{-3}$ M, respectively.

Back extractions were performed to test the reversibility of each extraction system. 1 M HNO_3 or 1 M NO_3^- were added to organic solutions, from which Rh(III) had been extracted using either DPPA or DPDTPA; the samples were then allowed to equilibrate for an additional 24 hours before the extraction was tested in these new conditions.

The B3LYP combination of density functionals was employed for the geometry optimization of the Rh(III) complex, $Rh(NO_3)_3$, and the extractant species $Rh(NO_3)_x(DPPA)_{3-x}$ and $Rh(NO_3)_x(DPDTPA)_{3-x}$ (x = 0 - 3) using the NWChem software package. The cc-pVDZ basis set was used to describe Rh(III) and the aug-cc-pVDZ basis set was used to describe all other atoms. In the case of Rh(III), this consists of segmented contracted 4s4p3d1f functions, along with a matching pseudopotential that replaces the 28 inner-shell ($[Ar]4s^2 3d^8$) electrons. Frequency calculations were performed on all optimized structures to obtain thermochemical corrections and ensure they correspond to a local minima.

The generalized equation for determining the binding energy of the extractant to the metal is represented by:

$$Rh(NO_3)_3 + xL^- \rightleftarrows Rh(NO_3)_{3-x} + xNO_3^-$$

where L^- is the conjugated base of phosphinic acid, HL, the binding extractant; H^+ was omitted for simplicity. Additional reaction schemes were considered, such that

$$Rh(NO_3)_3 + xL^- + n(H_2O) \rightleftarrows Rh(NO_3)_{3-x}(L)_x(H_2O)_n + xNO_3^-$$

where up to three water molecules bind to Rh(III), either causing the nitrate ions or extractant to bind mondentate.

III.c.2 Results and Discussion

It is hypothesized that Rh(III) extraction occurs through exchange of the acidic extractant proton and the nitrate ion originally bound to Rh(III). Assuming each phosphinic acid molecule displaces one NO_3^- ion to bind to Rh(III), the equilibrium constant for the reaction can be written as the extraction constant of the overall equilibrium:

$$K_{ex} = D\frac{[NO_3^-]^x[H^+]^x}{[HL]^x}$$

where *D* is the distribution coefficient, calculated as the Rh(III) concentration in the organic phase divided by the Rh(III) concentration in the aqueous phase. Taking the logarithm yields

$$logD = xlog[HL] - x\log[NO_3^-] - xlog[H^+] + logK_{ex}$$

Plots of *logD* as a function of *log[HL]*, *log[NO_3^-]*, or pH should provide a straight line with slope of x.

The pH of the samples after extraction for which the concentration of DPPA was varied remained stable after 7 hours of equilibration and remained unchanged after an additional 16 hours. The distribution ratio increased linearly with increasing extractant concentration, supporting the hypothesized reaction. The plot of *logD* as a function of *log[DPPA]* at constant pH , shown in Figure 4 (A), is a straight line with a slope of 0.96 (± 0.07), which suggests the binding of one DPPA molecule to one $Rh(NO_3)_3$ reactant.

Samples prepared to study the dependency of DPDTPA concentration showed that the pH stabilized after 7 hours of equilibration and did not change after 16 hours of additional contact time. A larger Rh distribution was observed for extractions performed with DPDTPA than with DPPA; for example, $1.9\cdot10^{-2}$ M DPDTPA yields an Rh(III) distribution ratio of 5.19 (± 0.07) while the same concentration of DPPA only yields a distribution ratio of 4.25. The plot of *logD* as a function of *log[DPDTA]* at constant pH (Figure 4 (B)) is linear with a slope of 0.98 (±0.05) suggesting that Rh(III) extraction by DPDTPA involves the complexation of one DPDTPA molecule by one Rh(III), as was the case for DPPA.

The Rh(III) extraction as a function of NO_3^- concentration was tested to determine the number of nitrate ions coordinated to each extracted Rh(III) complex. Rh(III) extraction decreases with an increasing NO_3^- concentration, as shown with Figure 5 (A).

A Rh(III) distribution ratio of 1.70 is observed in the presence of a NO_3^- concentration of $1.0 \cdot 10^{-3}$ M, but negligible Rh(III) extraction is measured in the presence of 1 M NO_3^-. The plot of *logD* as a function of *log[NO_3^-]* results in a straight line with a slope of -1.04 (± 0.06), suggesting the loss of a single nitrate ion during the complexation and subsequent extraction of Rh(III) by DPPA.

Figure 5. Influence of extractant concentration on the extraction of Rh(III). Aqueous phase: [Rh] = 5.3×10^{-4} M, [NO_3^+] = $1.5 \cdot 10^{-3}$ M, pH = 3.32; Organic phase: (A) DPPA in 1-pentanol. (B) DPDTPA in toluene.

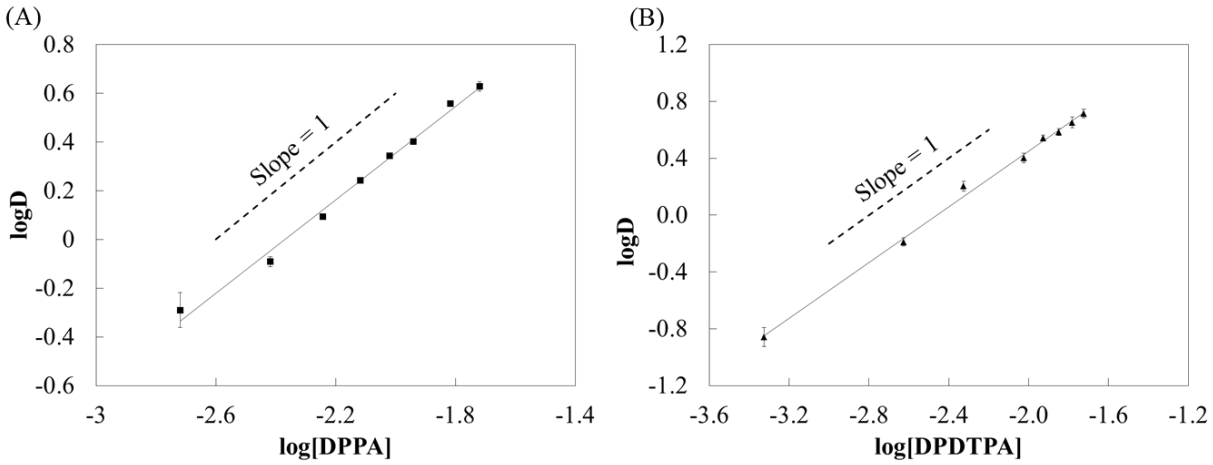

Figure 5 (B) demonstrates the decreased Rh(III) extraction by DPDTPA with increasing NO_3^- concentration. The Rh(III) distribution ratio drops from 2.143 to 0 as NO_3^- concentration increases from $2.5 \cdot 10^{-3}$ M to 1.0 M. The plot of *logD* as a function of *log[NO_3^-]* also yields a straight line with a slope of -1.03 (± 0.07), which suggests the loss of a single nitrate ion during Rh(III) extraction by DPDTPA.

As expected, Rh(III) extraction by DPPA decreases with an increasing HCl concentration (Figure 6 (A)), as the pH drops below the pKa of DPPA (2.32) causing a predominance of the protonated form of DPPA, which is less susceptible to undergo complexation with Rh(III). The distribution ratio drops from 1.24 to less than 0.01 if the HCl concentration increases from $1 \cdot 10^{-4}$ M to $1 \cdot 10^{-2}$ M. A reliable pH could not be determined for extraction solutions as the pH < 2, as it is not measureable with a standard pH electrode. The plot of *logD* as a function of *log[HCl]* is a straight line with a slope of -0.95 (± 0.06), which indicates that a single proton is exchanged during Rh(III) extraction by DPPA.

Figure 6. Influence of NO_3^- concentration on the extraction of Rh(III). Aqueous phase: [Rh(III)] = $5.3 \cdot 10^{-4}$ M, pH = 3.32; Organic phase: (A) [DPPA] = $1.9 \cdot 10^{-2}$ M in 1-pentanol (B) [DPDTPA] = $1.9 \cdot 10^{-2}$ M in toluene.

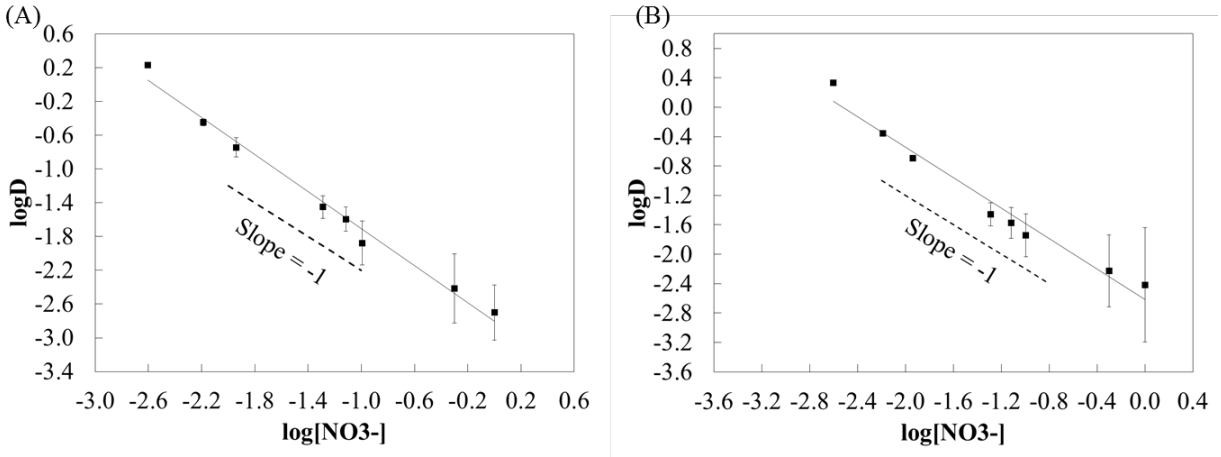

Figure 7. Influence of HCl concentration on the extraction of Rh(III). Aqueous phase: [Rh] = $5.3 \cdot 10^{-4}$ M in HCl, [NO_3^-] = $1.5 \cdot 10^{-3}$ M; Organic phase: (A) [DPPA] = $1.9 \cdot 10^{-2}$ M in 1-pentanol (B) [DPDTPA] = $1.9 \cdot 10^{-2}$ M in toluene.

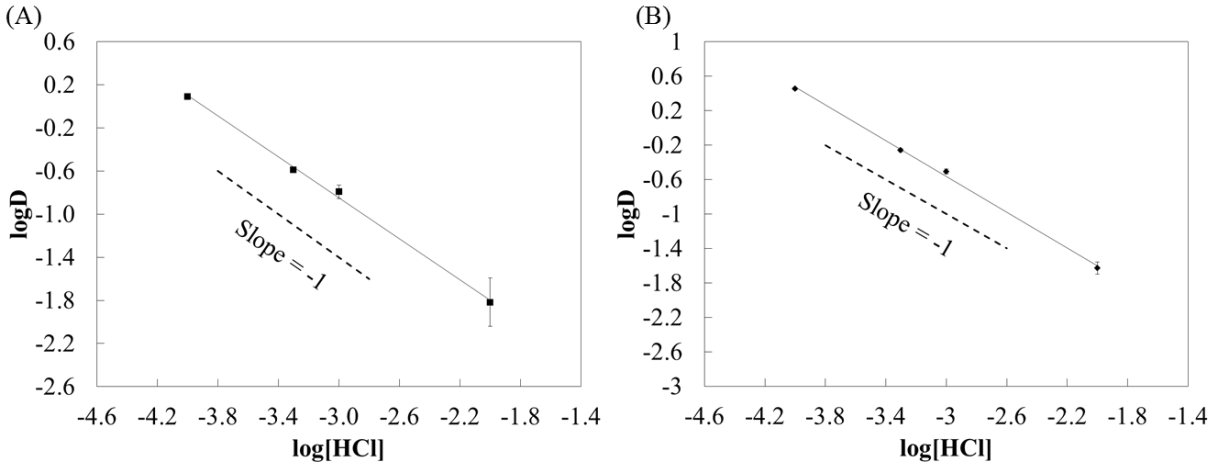

The pKa of DPDTPA, 2.70, is similar to that of DPPA. Therefore, we would expect DPDTPA to behave in a similar fashion as DPPA in the acid dependency study. Rh(III) extraction with DPDTPA should diminish with decreasing pH due to the formation of the protonated species that cannot extract Rh(III). Figure 6 (B) demonstrates a

decreased extraction with an increasing H^+ concentration. The plot of *logD* as a function of *log[HCl]* is a straight line with a slope of -1.03 (± 0.06), suggesting a single proton exchange during Rh(III) extraction by DPDTPA.

Data show negligible Rh(III) extraction if either NO_3^- or H^+ are present at 1 M or higher. Organic solutions obtained upon Rh(III) extractions with low concentrations of $NaNO_3$ or HNO_3 were subsequently used to test Rh(III) back-extractions; the results of which demonstrate that 99% (±1%) Rh(III) was stripped from the organic phases back into the aqueous phases upon addition of 1 M of either $NaNO_3$ or HNO_3. The ability to back-extract Rh(III) with NO_3^- or H^+ helps to validate the applicability and reversibility of the reaction.

The slope analysis results thus suggest that for both extraction systems

$$Rh(NO_3)_3 + \overline{HL} \rightleftarrows \overline{Rh(NO_3)_2(L)} + NO_3^- + H^+$$

and the extraction equilibrium expression becomes:

$$K_{ex} = D\,\frac{[NO_3^-][H^+]}{[HL]}$$

Using Eq. (6), the data lead to a K_{ex} = 4 (± 1)·10^{-5} for both DPPA and DPDTPA, and the free energy of extraction, ΔG_{ex}, at 298 K is calculated to be 24.98 (± 6.92) and 24.89 (± 2.95) kJ/mol for DPPA and DPDTPA, respectively. These data are unexpected as the Hard and Soft Lewis Acids and Bases (HSAB) principle would predict that DPDTPA would bind preferentially to Rh(III) because of the favorable interactions between the "soft" Rh(III) and sulfur coordinating atoms of DPDTPA than between Rh(III) and oxygen coordinating atoms of DPPA. Thus, the binding energies would be expected to be quite different due to the different donor groups present within the extractant, however, this is not observed experimentally based upon the overall free energy of the extraction. It is important, however, to recognize that ΔG_{ex} is a combination of several components, including the extractant binding, the energy barrier of the extracted product crossing from the aqueous phase to the organic phase, and the stability of the product in a given phase. Differences in the binding energies may exist, however these differences may be minimal compared to the energy associated in transport across the interface and/or the stability of the extracted products in the organic phase. Additionally, positive values of ΔG_{ex} indicate a non-spontaneous reaction at room temperature and suggest that a Le Châtelier type equilibrium is occurring wherein extraction is driven by the presence of excess ligand. Extractant concentrations must be two order greater than the concentration of Rh(III) to reach an 80% recovery from solution when Rh(III) is at millimolar concentrations.

The optimized geometries of the $Rh(NO_3)_x(L)_{3-x}$ (L = DPPA or DPDTPA, x = 0 - 3) were determined and key bond lengths are presented in Figure 8. Bond lengths remain relatively unchanged as the number of extractants bound to Rh(III) increases. To model extraction of Rh(III) by DPPA and DPDTPA, the following extractant addition reactions were considered:

$$Rh(NO_3)_3 + L^- \rightarrow Rh(NO_3)_2L + NO_3^- \quad (7)$$

$$Rh(NO_3)_2L + L^- \rightarrow Rh(NO_3)L_2 + NO_3^- \quad (8)$$

$$Rh(NO_3)L_2 + L^- \rightarrow RhL_3 + NO_3^- \quad (9)$$

The gas phase energies for each subsequent extractant binding (ΔG_{bind}) to Rh(III) becomes increasingly unfavorable. As shown in Table 2, the gas phase energy for the first extractant binding is unfavorable for both DPPA and DPDTPA. Note that the gas phase energetics will be in general significantly larger in magnitude than those in the solution phase, and thus it is the trend in values that is most relevant to the discussion here. Additions of a second and third extractant become increasingly unfavorable, indicating that these complexes would not be expected to form. This agrees with the experimental findings that only one extractant was determined to bind to Rh(III) in nitrate ion solutions and that the binding is not spontaneous at room temperature (298.15 K).

Figure 8. B3LYP/cc-pVDZ/aug-cc-pVDZ Optimized gas phase structures of the (A) $Rh(NO_3)_2$DPPA and (B) $Rh(NO_3)_2$DPDTPA extracted complexes with relevant bond distance shown (red atoms = O, dark blue = N, teal = Rh, orange = P, yellow = S, dark grey = C, white = H).

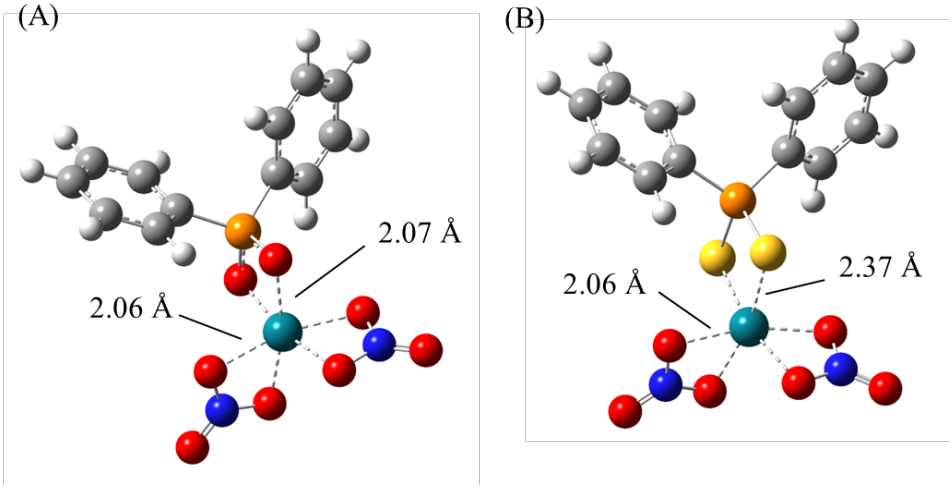

Table 6. Calculated gas-phase binding energies (in kJ/mol) for the addition of extractants to Rh(III).

Reaction	DPPA (ΔG_{bind})	DPDTPA (ΔG_{bind})
7	122	83.0
8	148	121
9	198	159

Perhaps more important is that the computationally determined binding energies, shown in Table 6, suggests an energetic difference between the two extractants. The calculated data indicates that DPDTPA should preferentially bind to Rh(III) over DPPA, as anticipated by HASB principle wherein the "softer" DPDTPA would be expected to bind stronger to the soft Rh(III). Yet the experimentally determined ΔG_{ex} does not coincide with the anticipated or calculated trends in phosphinic acid binding energies. This data then indicates that the dominant terms to ΔG_{ex} are likely those that correspond to the transport of the extraction complex from the aqueous:organic interface and or the stability of the extractant complex in the organic phase.

III.c.3 Conclusions

The extraction of Rh(III) from nitric acid solutions has been investigated using experimental and theoretical techniques. Experimental data indicates that extraction of Rh(III) using DPPA and DPDTPA is non-spontaneous at room temperature. The experimentally determined K_{ex} were similar for both extractants within error. Although these extractants show promises for application to spent nuclear fuel, there are discrepancies between theoretical and experimental data. Theoretical thermodynamic data presented suggests that larger differences in ΔG_{ex} should be observed based upon the binding energy of the extractant to the metal. Given that the experimental ΔG_{ex} values indicate no difference between the extractants, the dominant thermodynamic quantities associated with the extraction process are then presumed to be associated with the transport of the extraction complex from the aqueous:organic interface and or the stability of the extractant complex in the organic phase.

III.d Extraction of Rh(III) By Substitute Thiourea Ligands (2 manuscripts in preparation)

Using building blocks for ligands that were composed of thiourea groups, a suite of new ligands were proposed by CADME, with the top most "synthesizable" candidates being pursued for further study. These turned out to be various substituted benzoylthiourea ligands, whereupon N,N-diethyl-N'-benzoylthiourea was chosen by the Benny group for synthesis and further study. In the 1980s, benzoylthiourea ligands were shown to be able to remove PGMs from chloride media with near quantitative extraction as shown in Fig 9. Separation of PGMs from other base metals (Cu, Co, Ni) as well as isolation of Rh, Pd, and Ru in high purity was achieved through manipulation of pH, temperature, and chloride concentration. Best extraction results were seen at high temperatures ($T \geq 70°C$) with chloride concentrations greater than 2 M after 2-5 hours depending on ligand concentration. Additionally, di-alkyl benzoylthiourea ligands were observed to be more efficient than mono-alkyl or aromatic substituted ligands.

Figure 9. General scheme for the complexation of Rh(III) with N,N-diethyl-N'-benzoylthiourea.

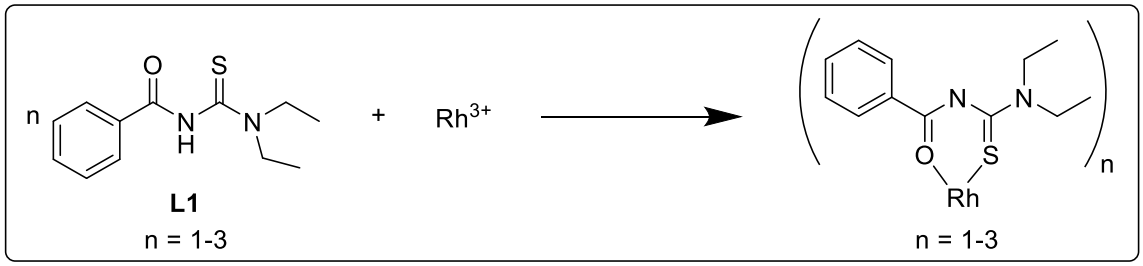

In this work, the first direct comparison of the extractability of rhodium(III) with N,N-diethyl-N'-benzoylthiourea (**L1**) from chloride and nitrate media is presented. Additional information about rhodium extraction with **L1** in nitrate media is necessary to determine the feasibility of rhodium recycling from dissolved SNF. Studies focused on room temperature extraction as high temperature processing of SNF for the recovery of fission product rhodium is not ideal. Effects of ligand concentration on the distribution ratio (D) were also studied to determine the extracted species.

III.d.1 Experimental Methods

All reagents and organic solvents were of reagent grade or better and used as purchased from Aldrich, Acros, or Fluka without further purification. N,N-diethyl-N'-benzoylthiourea (**L1**) was made as previously described. Rhodium starting material in the form of $RhCl_3 \cdot xH_2O$ was purchased from Pressure Chemical and $Rh(NO_3)_3 \cdot 2H_2O$ was purchased from Pfaltz and Bauer and were used without further purification. Rhodium stock solutions were made by dissolving the appropriate Rh starting material in 18 MΩ H_2O. Rh concentrations were determined by Inductively Coupled Plasma Optical Emission Spectrometry (ICP-OES) (Perkin Elmer Optima 3200 RL) and the instrument was calibrated with dilutions of a 1000 ppm Rh standard solution in 10% HCl (Acros Organics).

Liquid-liquid extraction experiments were performed in quadruplicate at room temperature with ligand concentrations of 0.005-0.05 M in 1-pentanol (1.0 mL) and standardized rhodium stocks (1.0 mL, 0.0005 M Rh) in sealed polypropylene tubes. In all cases, controls were run to verify the Rh did not adsorb to the extraction vessel. Room temperature extractions were rotated at 55 rpm for 1 or 7 days. The concentration of Rh in the aqueous phase was measured using ICP-OES. The distribution ratio (D) was calculated using the following equations:

$$D = \frac{[M]_{org}}{[M]_{aq,init}}$$

$$[M]_{org} = [M]_{aq,init} - [M]_{aq}$$

where $[M]_{aq,\ init}$ and $[M]_{aq}$ are the initial and final concentrations of metals ions, respectively, in the aqueous phase.

III.d.2 Results and Discussion

Extraction studies were carried out on a rotator that completely inverts samples (55 rpm) at room temperature. Standardized rhodium solutions ([Rh] = 5.0×10^{-4} M for nitrate and chloride media) were made in 18 MΩ H_2O to ensure that no extra ions were introduced into the media that would affect the speciation of $RhCl_3 \bullet xH_2O$; which, when dissolved in ultra-pure water, has been shown to be a mixture of $[Rh(OH_2)_4Cl_2]Cl$ and $Rh(OH_2)_3Cl_3$. 1-pentanol was used as the organic phase to provide a more polar interface than other hydrocarbon organic solvents (e.g., toluene, chloroform). Rhodium extraction with **L1** was examined at two time points: 1 day as a comparison to previous work, and 7 days as the kinetics of Rh(III) are very slow.[5, 22-24] At each time point, the $[Rh]_{(aq)}$ was analyzed by ICP-OES to determine the distribution ratio (D) within the layers.

In chloride media, D at 1 day ranged from 0.09 ± 0.04 (8%) to 0.31 ± 0.04 (23%) when varying the concentration of **L1** from 0.005 to 0.05 M. At high ligand concentrations (0.05 M), an increase in extraction time from 1 to 7 days afforded a significant increase in distribution ratios from 0.31 ± 0.04 to 15.4 ± 0.08 (94% extraction), respectively (Fig. 10). These results are consistent with extractions done in chloride media with similar benzoylthiourea ligands at high temperature (70°C). However, **L1** in this study demonstrated increased distribution ratios at lower $[Cl^-]$ compared to previous studies.

Table 7. Distribution ratios for $RhCl_3$ extraction.

Time (d)	[L1] (M)	D (org/aq)
1	0.005	0.09 ± 0.04
	0.025	0.17 ± 0.02
	0.050	0.31 ± 0.04
7	0.005	0.40 ± 0.02
	0.025	5.21 ± 0.09
	0.050	15.4 ± 0.8

Figure 10. Distribution ratios for $RhCl_3 \cdot xH_2O$ extraction with **L1**

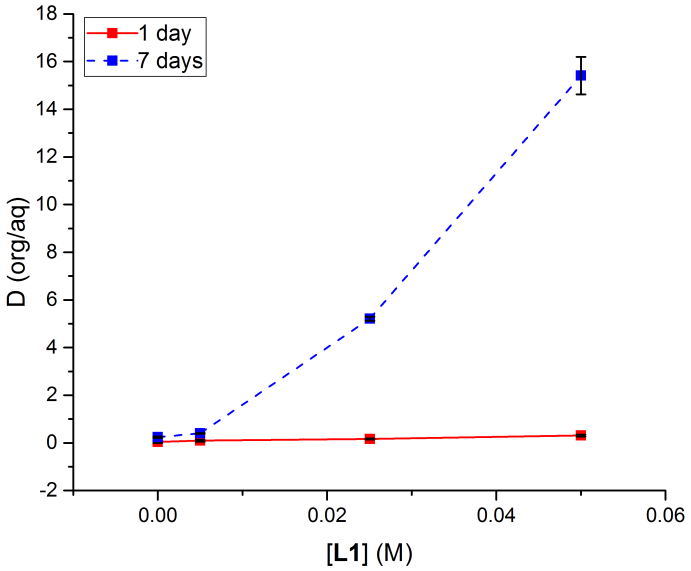

In nitrate media, the distribution ratios at 1 day were significantly higher than chloride media ranging from 0.39 ± 0.08 (28%) to 0.57 ± 0.08 (36%) with varying concentrations of **L1** from 0.005 to 0.05 M, respectively. When the extraction time was increased to 7 days, D generally increased across the concentration range. Quantitative extraction was observed in nitrate media at higher ligand concentrations (0.025 M, D = 51.4 ± 5.5 (98%) and 0.05 M, D = 130.2 ± 6.0 (99%)) (Fig. 11). In comparison with chloride media 7 day extraction experiments, similar concentrations yielded a significantly lower D values. For example, at 0.025 M under chloride conditions D = 5.21 ± 0.09 (84%), whereas under nitrate media quantitative extraction was observed. These results indicate the improved extraction efficiency of rhodium from nitrate over chloride media. While these studies were conducted at room temperature, previous studies with chloride media indicate improved rhodium extraction efficiency with increased temperatures. This effect may also be applicable for the extraction of rhodium in nitrate media.

Table 8. Distribution ratios for $Rh(NO_3)_3$ extraction.

Time (d)	[L1] (M)	D (org/aq)
1	0.005	0.39 ± 0.08
	0.025	0.45 ± 0.08
	0.050	0.57 ± 0.08
7	0.005	0.20 ± 0.01
	0.025	51.4 ± 5.5
	0.050	130.2 ± 6.0

Figure 11. Distribution ratios for $Rh(NO_3)_3$ extraction with **L1**.

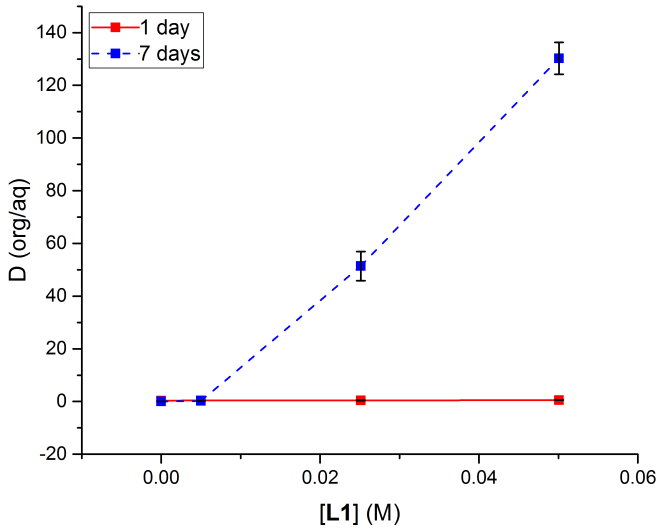

The concentration dependency of the extraction, evaluating different metal to ligand ratios (M:L), was conducted on the 7 day extraction data for both chloride and nitrate media. Previous work with chloride media did not determine the extracted species, but assumed three ligands were required to extract the rhodium complex. To determine the number of ligands coordinated to the metal, slope analysis (log D vs log [**L1**], Fig. 12) was conducted on media systems. The chloride media indicated an M:L of 2:3 possibly suggesting the extraction of potential bridging rhodium dimeric complexes ($Rh_2Cl_9^{3-}$)[10, 13, 26] or a bridging ligand molecule between two rhodium centers. As the ligands complex sequentially, the addition of a second ligand to the primary coordination sphere yields the formation of the *cis* and *trans* isomers (Fig. 13). The *trans* isomer must undergo ligand rearrangement to the *cis* isomer to accommodate three ligands on the metal center. If ligand rearrangement and anion dissociation is energetically unfavorable, formation of the tris ligand product may be hindered in chloride media. Conversely, nitrate media analysis provided an uncomplicated M:L of 1:3 indicating that the extracted species was fully saturated with three ligands in the coordination sphere. This result confirms the facile substitution of the nitrates by stronger coordinating ligands in comparison to the chloride system.

Figure 12. Slope analysis of $RhCl_3$ and $Rh(NO_3)_3$ extraction at 7 days.

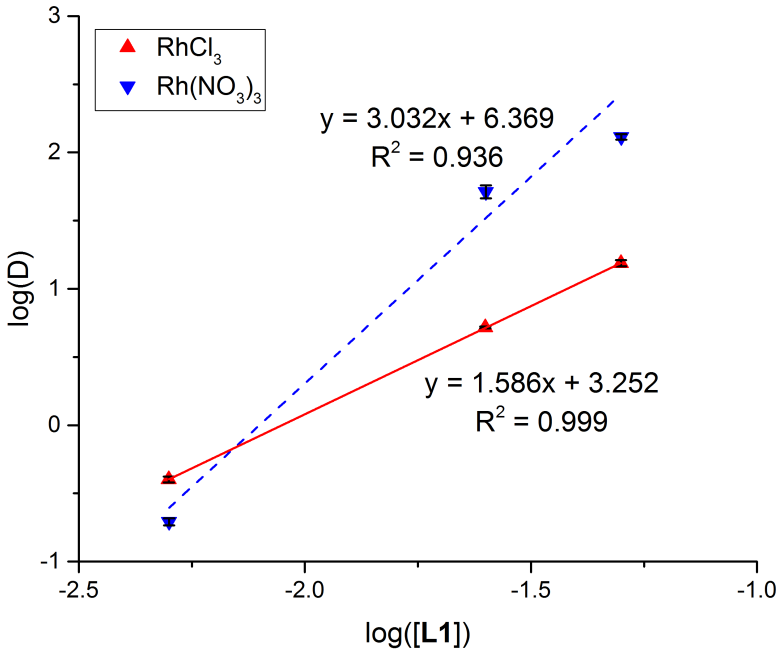

Figure 13. Proposed speciation for rhodium extraction.

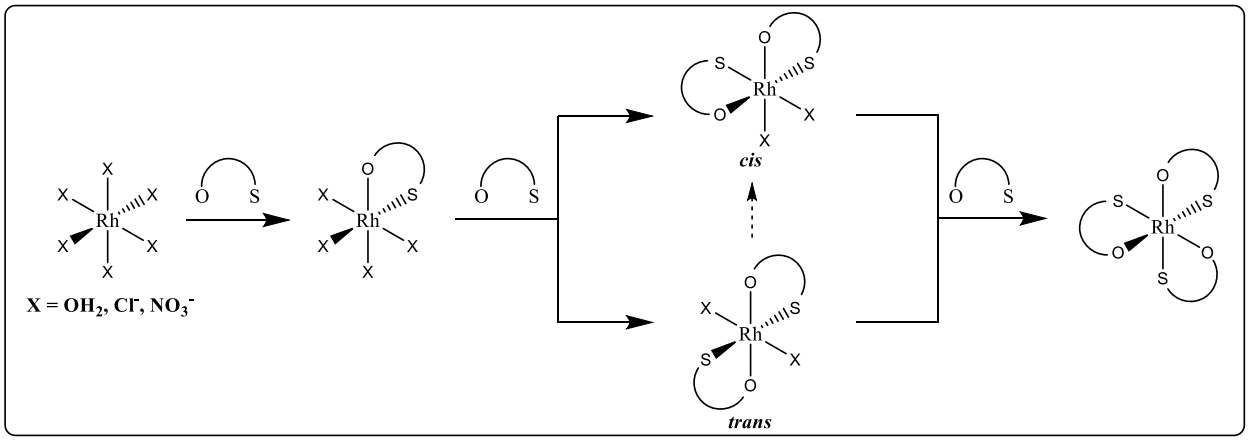

III.d.3 Conclusions

This is the first direct comparison of the extractability of rhodium(III) from chloride and nitrate media with a benzoylthiourea ligand. Extraction of rhodium from nitrate media had significantly improved distribution ratios than chloride media with lower ligand

concentrations. Slope analysis revealed different coordination species were extracted in chloride vs. nitrate media. Addition of the third ligand appeared more favorable to yield the Rh(**L1**)$_3$ complex in nitrate media. Overall, the extraction of rhodium(III) performed significantly better in nitrate media over chloride media and provided straightforward understanding of the extraction speciation.

IV. Summary

A software program (CADME) has been developed that interfaces with the HostDesigner software so as to read in large databases of ligands that may act as potential extractants. It is then interfaced with NWChem to launch in parallel a series of energy or optimization calculations and to determine key parameters associated with ligand reorganization and binding strength, filtering the database of ligands into a series of ligands that can be tested experimentally. This first version of CADME cannot account for any solution-phase interactions or forces that may influence the distribution coefficient of a metal ligand complex, however CADME is ongoing further development to be interfaced with classical molecular dynamics simulation software. At the same time, fundamental studies of Rh(III) speciation was pursued to understand the nature of the reacting species with an extracting ligand in both chloride and nitrate media. Then, known extractants were studied with Rh(III), specifically phosphonic acids, whereupon it was determined that for those extractants the driving force for the extraction was NOT metal-ligand complexation but rather the transport process across the phase boundary. This shed light on the importance for CADME to account for solvation differences in the aqueous versus the organic phases and not only the favorability of ligand complexation. A series of substituted thiorurea based ligands was determined by CADME to have favorable complexation properties for Rh(III) and the ligand N,N-diethyl-N'-benzoylthiourea was synthesized and its extraction properties were pursued under different solution phase conditions. We believe that these initial studies and the software development of CADME provides an excellent platform for future development of novel solvent extraction systems for Rh(III).